Analytical Footprints: Compact Representation of Elementary Singularities in Wavelet Bases

4 authors, including:

Dimitri Van De Ville
École Polytechnique Fédérale de Lausanne
678 PUBLICATIONS   **10,658** CITATIONS

SEE PROFILE

Brigitte Forster-Heinlein
Universität Passau
52 PUBLICATIONS   **610** CITATIONS

SEE PROFILE

Michael Unser
École Polytechnique Fédérale de Lausanne
969 PUBLICATIONS   **41,091** CITATIONS

SEE PROFILE

Some of the authors of this publication are also working on these related projects:

Image Reconstruction Algorithms View project

Real time 3-D intracellular nanomanipulator View project

Analytical Footprints: Compact Representation of Elementary Singularities in Wavelet Bases

Dimitri Van De Ville, *Member*, Brigitte Forster-Heinlein, *Member*,
Michael Unser, *Fellow*, Thierry Blu, *Senior Member*

Abstract—We introduce a family of elementary singularities that are point-Hölder α-regular. These singularities are self-similar and are the Green functions of fractional derivative operators; i.e., by suitable fractional differentiation, one retrieves a Dirac δ function at the exact location of the singularity. We propose to use fractional operator-like wavelets that act as a multiscale version of the derivative in order to characterize and localize singularities in the wavelet domain. We show that the characteristic signature when the wavelet interacts with an elementary singularity has an asymptotic closed-form expression, termed the analytical footprint. Practically, this means that the dictionary of wavelet footprints is embodied in a single analytical form. We show that the wavelet coefficients of the (non-redundant) decomposition can be fitted in a multiscale fashion to retrieve the parameters of the underlying singularity. We propose an algorithm based on stepwise parametric fitting and the feasibility of the approach to recover singular signal representations.

Index Terms—Elementary singularities, Footprints, Wavelet Bases, Generalized Fractional Splines, Fractional Derivatives

I. INTRODUCTION

WAVELET bases provide an elegant decomposition of $L^2(\mathbb{R})$, the space of square integrable functions [1], [2]. Various applications take advantage of the wavelet representation; e.g., data compression, denoising, and analysis of singularities [3]. For a biorthogonal wavelet system, it is well known that the order of approximation of the scaling function at the synthesis side imposes the number of vanishing moments—and thus the differentiation order—of the wavelet at the analysis side. The differentiator behavior has direct consequences for applications. First, transient features such as discontinuities are characterized by wavelet coefficients in their neighborhood only, which is consistent with the derivative-like behavior. Second, the smooth parts of the signal get filtered out and transfered to the lowpass subband that is subsampled coarsely. Mallat and colleagues [4]–[6] used wavelets to recover a characteristic representation of the

signal from its wavelet coefficients' zero-crossings (when the wavelet acts like a second-order derivative) or their modulus maxima (when it acts like a first-order derivative). Due to the lack of shift-invariance of the wavelet transform, Mallat and Zhong [5] proposed a redundant and nonorthogonal version, thus extending wavelet bases to wavelet frames. This transform was later also studied by Wang [7]. While the redundant wavelet transform makes the analysis of the coefficients easier, it brings along an important disadvantage, next to redundancy, which is the non-uniqueness of the synthesis step.

Characterization in terms of elementary singularities (e.g., spikes, jumps, or discontinuities of the derivatives) is one way to model signals. Mathematically, the behavior of elementary singularities can be characterized by their Lipschitz (or Hölder) exponent α, which can be infered from the rate of decay of its wavelet coefficients as the scale s decreases:

$$\left| \left\langle f(\cdot), \sqrt{s^{-1}} \psi(\cdot/s - k) \right\rangle \right| \le A s^{\alpha + 1/2}.$$

It also is the key property behind the concept of the cone of influence of a singularity over scale [6]. Modeling in terms of singularities is especially relevant for field of seismic exploration, where the detection of different layers in the underground can be formulated as a "sparse spike deconvolution" problem [3, Sect. 13.3.2]. Here, the underlying signal is assumed to be a sum of spikes, measured through the seismic wavelet. In that case, it appropriate to impose the sparsity constraint using ℓ^1 minimization on the signal representation in the Dirac basis [8], [9]. The spike model can also be extended; for example, the Lipschitz exponent has been obtained using the continuous wavelet transform in order to measure local sharpness of the reflectors [10] or by investigating the effect of the singularity on the continuous wavelet [11]. This type of approach has also been pursued using discrete B-spline bases that are tuned to a large class of singularities [12]. Singularities and their multiscale properties have been used in other fields as well such as for the detection of characteristic points in ECG signals [13] or to perform step detection and estimation using multiscale products [14]. More recently, Dragotti and Vetterli proposed "wavelet footprints" as atoms that explicitly characterize signal jumps and that constitute a dictionary [15]; these footprints need to be learned from wavelet decompositions and become shift-variant in the case of wavelet bases. The requirement of learning the wavelet footprint comes from the fact that the mother wavelet of a discrete wavelet transform is often only known implicitly and does not have a tractable analytical expression

(e.g., Daubechies' wavelet are defined by the iterated filter relation). Bruni and Vitulano proposed a practical scheme for more general singularities that is also capable of resolving overlapping footprints [16].

In this paper, we do not consider an explicit dictionary, but we derive a closed-form analytical footprint of the elementary singularity in a well-chosen wavelet basis—retrieving the singularities from their wavelet decomposition then becomes a parametric fitting problem. As a starting point, we consider the fractional derivative/integral operator ∂_τ^γ, where the order γ and the phase τ can both be real-valued. Elementary singularities are then introduced as the Green functions ρ of the derivative operator ∂_τ^γ, for $\gamma \geq 0$; i.e., they satisfy $\partial_\tau^\gamma \{\rho\} = \delta$. Equivalently, they can be interpreted as the impulse response of the fractional integral operator $\partial_\tau^{-\gamma}$. Next, we consider the family of semi-orthogonal fractional B-spline wavelet bases [17], [18] associated to ∂_τ^γ, $\gamma \geq 1$, which have also been used for layer detection in seismic exploration [12]. We focus on a particular wavelet within this family, termed the "operator wavelet," for which we derive an explicit closed-form expression together with its fractional integrals that model the interaction of the wavelet with an elementary singularity. This allows us to generate the atoms of a dictionary without explicit learning; i.e., our analytical footprint contains all the information. The operator wavelet also has the attractive property that the wavelet coefficients within a basis decomposition of these singularities are mono- or bimodal only.

This paper is organized as follows. In Sect. II, we start by revisiting fractional derivatives and the associated singularities. Then, in Sect. III, we propose the design procedure for the operator wavelet and we investigate its main properties. We also characterize the wavelet and its fractional integrals, which leads to the definition of the analytical wavelet footprint. In Sect. IV, we demonstrate how to use these footprints with a practical stepwise parametric fitting algorithm that properly separates the singular and smooth parts of a signal.

Notations

We define the conventional inner product between two L_2 functions f_1 and f_2 as

$$\langle f_1, f_2 \rangle = \int_{-\infty}^{\infty} f_1(x) f_2^*(x) \mathrm{d}x, \tag{1}$$

where * denotes the complex conjugate. The associated Euclidean norm is $||f||_{L_2}^2 = \langle f, f \rangle$. The Fourier transform of f is defined as

$$\hat{f}(\omega) = \int_{-\infty}^{\infty} f(x) e^{-j\omega x} \mathrm{d}x. \tag{2}$$

For sequences in ℓ_2, we define the inner product

$$\langle h_1, h_2 \rangle_{\ell_2} = \sum_{k \in \mathbb{Z}} h_1(k) h_2^*(k). \tag{3}$$

The z-transform of a sequence $h \in \ell^2$ is denoted by

$$H(z) = \sum_{k \in \mathbb{Z}} h[k] z^{-k}, \tag{4}$$

while the corresponding Fourier transform is $H(e^{j\omega})$. We define the fractional power of a complex variable z as $z^\alpha = |z|^\alpha e^{j\alpha \arg(z)}$ with $j = \sqrt{-1}$ and $\arg(z) \in [-\pi, \pi[$. When we omit the range for integrals and summations, they should be understood as over $\mathbb{R}$ and $\mathbb{Z}$, respectively.

II. FRACTIONAL DERIVATIVES AND ELEMENTARY SINGULARITIES

Fractional derivative/integral operators are a long-standing research topic in mathematics [19]–[22] with many applications in physics, for example [23]. These operators can be introduced in various ways [24], [25]; here, we define them in the sense of distributions by the Fourier-domain formulation:

$$\partial_\tau^\gamma f(x) = \int_{-\infty}^{\infty} \underbrace{(-j\omega)^{\frac{\gamma}{2}-\tau} (j\omega)^{\frac{\gamma}{2}+\tau}}_{=: \hat{\partial}_\tau^\gamma(\omega)} \hat{f}(\omega) e^{j\omega x} \frac{\mathrm{d}\omega}{2\pi}, \tag{5}$$

where $\gamma \in \mathbb{R}$ is the order and $\tau \in \mathbb{R}$ is the phase parameter. We also notice that the Fourier representation of the time-reversed (or adjoint) operator $\overline{\partial}_\tau^\gamma = \partial_{-\tau}^\gamma$ corresponds to the $\hat{\partial}_\tau^\gamma(-\omega)$. The fractional derivative/integral operators form a complete family of scale-invariant convolution operators [26].

Definition 1 (Elementary singularity): The elementary singularity $\rho_\tau^\gamma(x)$ of order γ and phase shift τ is the Green function of the operator ∂_τ^γ:

$$\partial_\tau^\gamma \rho_\tau^\gamma(x) = \delta(x). \tag{6}$$

These Green functions can be determined by inverse Fourier transformation and are given by

$$\rho_\tau^{\gamma+1}(x) = \begin{cases} C_\tau^\gamma |x|^\gamma + D_\tau^\gamma |x|^\gamma \log |x|, & \gamma \text{ is odd} \\ C_\tau^\gamma |x|^\gamma \log |x| + D_\tau^\gamma |x|^\gamma \operatorname{sign}(x), & \gamma \text{ is even} \\ C_\tau^\gamma |x|^\gamma + D_\tau^\gamma |x|^\gamma \operatorname{sign}(x), & \text{otherwise} \end{cases} \tag{7}$$

where C_τ^γ and D_τ^γ are suitable constants [27, ch. 2], [28, pp. 257f], [22, pp. 16–17], [29], [18].

The prototypical example is the unit step function $u(x) = \rho_{1/2}^1 = (x)_+^0$, which is such that $\mathrm{D}u(x) = \delta(x)$ where $\mathrm{D} = \partial_{1/2}^1$ is the ordinary derivative operator. Thanks to the scale-invariance of the associated operators, each Green function is self-similar in the sense that $\rho_\tau^\gamma(x/T) = \lambda \rho_\tau^\gamma(x)$ with $\lambda = T^{1-\gamma}$. In Figure 1, we show several subsets of our family of elementary singularities. For first-order singularities, they vary from the unit step to the spike, as shown in (a). Higher-order singularities characterize discontinuities of a corresponding γ-th order fractional derivative. Notice that the signal ρ_τ^γ has precisely one singularity at the origin with a Lipschitz exponent $\gamma - 1$ [17].

Definition 2 (Singular signal model): A signal is said to be singular if it is a finite sum of weighted elementary singularities plus a smooth term that is C^∞.

Specifically, we express a singular signal containing M singularities of orders $\gamma_m \geq 0$, and with phase parameters τ_m as a sum of the elementary singularities $\rho_{\tau_m}^{\gamma_m}$ and the smooth part $f_0(x)$:

$$f(x) = \sum_{m=1}^{M} a_m \rho_{\tau_m}^{\gamma_m}(x - x_m) + f_0(x), \tag{8}$$

where the continuously-defined parameters are the amplitudes a_m, $m = 1, \ldots, M$, and the positions $x_m \in \mathbb{R}$.
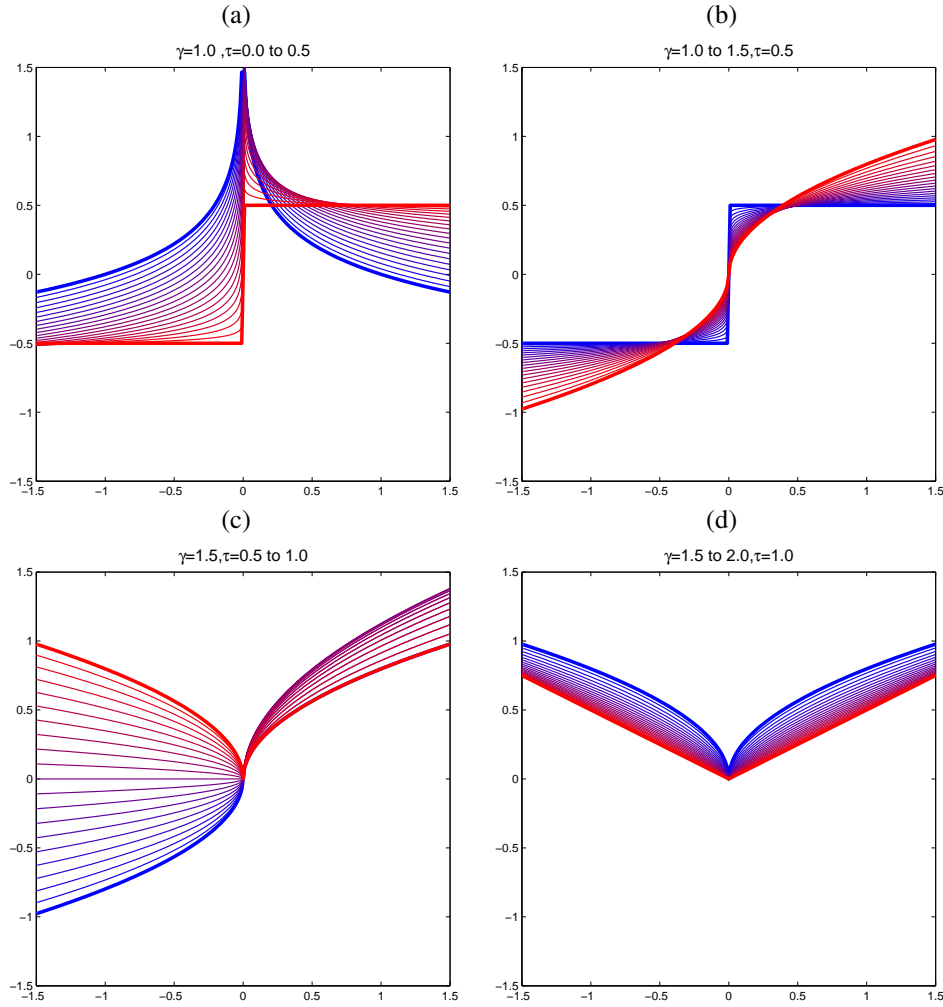
(a)

$\gamma=1.0$,$\tau=0.0$ to 0.5

(b)

$\gamma=1.0$ to 1.5,$\tau=0.5$

(c)

$\gamma=1.5$,$\tau=0.5$ to 1.0

(d)

$\gamma=1.5$ to 2.0,$\tau=1.0$

Fig. 1. Family of elementary singularities associated to the fractional derivative operator ∂_τ^γ. Several subsets of singularities are shown in (a)-(d). The sweep-through starts in blue and ends in red.

III. OPERATOR WAVELETS

A. Fractional (α, τ)-Splines and Wavelets

Closely related to the fractional derivative operators are the fractional B-splines of degree $\alpha \geq 0$ ($\alpha \in \mathbb{R}$) and phase parameter $\tau \in \mathbb{R}$. These are most conveniently defined in the Fourier domain as

$$\hat{\beta}_\tau^\alpha(\omega) = \left(\frac{1 - e^{j\omega}}{-j\omega} \right)^{\frac{\alpha+1}{2} - \tau} \left(\frac{1 - e^{-j\omega}}{j\omega} \right)^{\frac{\alpha+1}{2} + \tau}. \quad (9)$$

This family of B-splines contains the traditional symmetric ($\tau = 0$) and causal ($\tau = (\alpha + 1)/2$) B-splines. The Fourier domain definition of the B-spline can also be written as

$$\hat{\beta}_\tau^\alpha(\omega) = \frac{\hat{\Delta}_\tau^{\alpha+1}(e^{j\omega})}{\hat{\partial}_\tau^{\alpha+1}(\omega)} \quad (10)$$

where the numerator

$$\hat{\Delta}_\tau^{\alpha+1}(z) = (1 - z)^{\frac{\alpha+1}{2} - \tau}(1 - z^{-1})^{\frac{\alpha+1}{2} + \tau} \quad (11)$$

is the z-transform of the fractional finite difference operator Δ_τ^γ of order γ (convergence limited to the unit circle $z = e^{j\omega}$). We can interpret the B-spline as the application of the localization operator $\Delta_\tau^{\alpha+1}$ to the elementary singularity; i.e., $\beta_\tau^\alpha = \Delta_\tau^{\alpha+1} \rho_\tau^{\alpha+1}(x)$ [30].

The (α, τ)-splines satisfy the (dyadic) two-scale relation where the scaling filter $h[k]$ relates B-splines at two consecutive scales as

$$\beta_\tau^\alpha \left(\frac{x}{2} \right) = \sqrt{2} \sum_k h[k] \beta_\tau^\alpha(x - k) \quad (12)$$

whose z-transform is given by

$$\begin{aligned} H(z) &= 2^{-\alpha - \frac{1}{2}} \frac{\hat{\Delta}_\tau^{\alpha+1}(z^2)}{\hat{\Delta}_\tau^{\alpha+1}(z)} \\ &= 2^{-\alpha - \frac{1}{2}}(1 + z)^{\frac{\alpha+1}{2} - \tau}(1 + z^{-1})^{\frac{\alpha+1}{2} + \tau} \\ &= 2^{-\alpha - \frac{1}{2}} \hat{\Delta}_\tau^{\alpha+1}(-z). \end{aligned} \quad (13)$$

The autocorrelation filter of these splines is written in the Fourier domain as

$$A(e^{j\omega}) = \sum_k \left| \hat{\beta}_\tau^\alpha(\omega + 2\pi k) \right|^2. \quad (14)$$

The associated approximation spaces $\mathcal{V}_i$ at a (dyadic) scales $i \in \mathbb{Z}$ are specified as

$$\mathcal{V}_i = \text{span} \left\{ \sqrt{2^{-i}} \beta_\tau^\alpha \left(2^{-i} x - k \right) \right\}_{k \in \mathbb{Z}}, \quad (15)$$

and the wavelet spaces

$$\mathcal{W}_i = \text{span}\left\{\sqrt{2^{-i}}\psi(2^{-i}x - k)\right\}_{k\in\mathbb{Z}}, \qquad (16)$$

can be constructed as the orthogonal complement between two subsequent approximation spaces; i.e., $\mathcal{W}_i \oplus_\perp \mathcal{V}_i = \mathcal{V}_{i-1}$. The construction of a proper wavelet basis is summarized in the following proposition.

Proposition 1: For any given fractional B-spline β_τ^α, one can specify a corresponding semi-orthogonal spline wavelet ψ, parametrized by some bounded filter $Q(z)$. The following properties apply.

(i) The wavelet is characterized by the relation

$$\psi\left(\frac{x}{2}\right) = \sqrt{2}\sum_k w[k]\beta_\tau^\alpha(x - k), \qquad (17)$$

where $w[k]$ is the so-called wavelet filter. The Fourier domain counterpart is

$$\hat{\psi}(2\omega) = W(e^{j\omega})\frac{\hat{\beta}_\tau^\alpha(\omega)}{\sqrt{2}}, \qquad (18)$$

where $W(z) = z^{-1}Q(z^2)H(-z^{-1})A(-z)$;

(ii) The wavelet generates a Riesz basis whenever $Q(e^{j\omega})$ is bounded by $C_0 \le |Q(e^{j\omega})| \le C_1$ for some positive constants $0 < C_0, C_1 < \infty$;

(iii) At low frequencies, the wavelet follows the behavior of the associated derivative operator:

$$\hat{\psi}(\omega) \propto \hat{\partial}_\tau^\gamma(-\omega)e^{-j\omega/2} + O(|\omega|^{\gamma+1}), \quad \text{as } \omega \to 0. \ (19)$$

For the proof see App. B.

Proposition 1 (iii) shows that for any valid polynomial $Q(z^2)$, the corresponding wavelet behaves as a fractional derivative operator. Therefore, analyzing a signal $f(x)$ with this wavelet yields samples of the operator ∂_τ^γ applied to a smoothed version of the input signal:

$$\langle f(\cdot), \psi(\cdot - k)\rangle = \partial_\tau^\gamma\{\phi * f\}(k), \qquad (20)$$

where the smoothing function is formally defined in the Fourier domain as $\hat{\phi}(\omega) = \hat{\psi}(\omega)/\hat{\partial}_\tau^\gamma(-\omega)$. The key point is that $\hat{\phi}(0)$ is well-defined and non-vanishing because of (19).

When α is integer, and $\tau = 0$, one obtains the classical "symmetric B-spline wavelet" by setting $Q(z) = 1$, which corresponds to the wavelet filter $W(z)$ with the shortest possible support [31]:

$$W(z) = z^{-1}H(-z^{-1})A(-z). \qquad (21)$$

It is also possible to select $Q(z)$ to obtain the well-known (orthogonal) Battle-Lemarié wavelets [32].

B. Operator Wavelets

In this paper, we are interested in one particular fractional spline wavelet: the operator-like wavelet.

Theorem 1: The operator wavelet ψ for the fractional B-spline scaling function of order $\gamma = \alpha + 1$ and phase parameter τ corresponds to

$$\psi\left(\frac{x}{2}\right) = \overline{\partial}_\tau^\gamma \beta_{\text{int}}^{2\gamma-1}(x - 1), \qquad (22)$$

where $\beta_{\text{int}}^{2\gamma-1}$ is the symmetric 2γ-th order interpolating B-spline. The operator wavelet has the following attractive properties:

(i) it closely matches the derivative operator in the Fourier domain as shown by its Taylor development

$$\hat{\psi}(\omega) \propto \hat{\partial}_\tau^\gamma(-\omega)e^{-j\omega/2} + O(|\omega|^{3\gamma}), \quad \text{as } \omega \to 0; \ (23)$$

which has a much smaller residual than (19).

(ii) the wavelet and its fractional integrals have an asymptotic analytical form

$$\partial_{-\tau_0}^{-\gamma_0}\psi(x) \to \frac{\pi^{\gamma-\gamma_0+1}}{4\gamma}\text{Re}\underbrace{\left[\frac{e^{j\pi(x-(\tau+\tau_0))}}{\sin\left(\frac{\pi(\gamma-\gamma_0)}{4\gamma} + j\frac{\pi^2(2x-1)}{4\gamma}\right)}\right]}_{g(x;\gamma,\tau,\gamma_0,\tau_0)}. \ (24)$$

for $x \to 0$ where $\gamma_0 < \gamma$. The limiting form improves as the order $\gamma = \alpha + 1$ increases.

For the proof see App. C.

The form (22) of the operator wavelet deserves some further analysis. As the fractional derivative operator acts on the smoothing function that is an interpolating B-spline of twice of the order γ, the γ-th derivative of a spline of order 2γ results in a spline of order γ, thus ensuring that the wavelet is contained in the span of the scaling function at the next finer scale. In fact, the operator wavelets coincide with the "cardinal spline wavelets" that were proposed by Chui and Wang [33] for causal B-spline of integer order. Here, we are proposing an extension to fractional operators (fractional orders and shifts). The fact that this construction improves the operator-like behavior of the wavelet does seem to have been emphasized before. The limiting form of the operator wavelet is also an original contribution of this work.

We should also note that there are other instances in the literature that are relying on an equation similar to (22); i.e., obtaining the wavelet by applying the operator to the interpolant of the "augmented order" function space, especially in higher dimensions. Micchelli *et al.* [34] proposed this construction for polyharmonic wavelets in any number of dimensions and for dyadic subsampling; these wavelets are related to the (iterated) Laplacian operator. This concept of wavelet design has also been generalized for almost any differential operator [35], including for Wirtinger-type operators [36], [37] and Riesz transforms [38].

Coming back to the fractional splines, we now show some examples where we compare the B-spline wavelets and the operator ones. In these comparisons, we assume that both wavelets are scaled in the same way. For these illustrations, we rescale the B-spline wavelet such that the frequency response for $\omega \to 0$ matches the derivative operator.

We start by noting that the B-spline wavelets and operator wavelets coincide for $\alpha = 0$. In Fig. 2 (a), we show the frequency response of both wavelets together with that of the corresponding derivative operator. For $\alpha > 0$, the operator wavelet matches the operator behavior more closely than the B-spline wavelet does. The examples in Fig. 2 (b)-(d) illustrate how the operator wavelets coincide with the pure derivative operator in the Fourier domain over a large range of ω. These

plots hold for every shift τ. It is also interesting to plot the wavelets in the spatial domain. In Fig. 3 (a), the symmetric wavelets for $\alpha = 1$ (i.e., the "linear" wavelets) are shown. The operator wavelet has a theoretical infinite support but stays in practice very similar to the B-spline wavelet. For higher degrees, such as $\alpha = 2.5$ as shown Fig. 3 (b), the difference between both wavelets becomes more significant.

C. Filterbank Implementation

As usual, we introduce the subscript notations for the scaling function and wavelets as $\varphi_{i,n}(x) = 2^{-i/2}\varphi(x/2^i - n)$ and $\psi_{i,n}(x) = 2^{-i/2}\psi(x/2^i - n)$, respectively. Each signal $f(x)$ of $\mathcal{V}_0$ can be expanded uniquely as a sum of two parts coming from $\mathcal{V}_1$ and $\mathcal{W}_1$. Iterating the expansion J times results into the decomposition

$$f(x) = \sum_{n \in \mathbb{Z}} c_{(J)}[n]\varphi_{J,n}(x) + \sum_{i=1}^{J} \sum_{n \in \mathbb{Z}} d_{(i)}[n]\psi_{i,n}(x), \quad (25)$$

where the coefficients $c_{(i)}[n]$ and $d_{(i)}[n]$ are determined as the projection of the signal in the subspaces; i.e., we have $c_{(i)}[n] = \langle f, \tilde{\varphi}_{i,n} \rangle$ and $d_{(i)}[n] = \langle f, \tilde{\psi}_{i,n} \rangle$, where $\tilde{\varphi}$ and $\tilde{\psi}$ are the dual scaling function and dual wavelet. The dual function $\tilde{\varphi}$ is the unique function in $\mathcal{V}_0$ that satisfies $\langle \tilde{\varphi}_{0,k}, \varphi_{0,l} \rangle = \delta_{k-l}$.

In practice, the wavelet decomposition algorithm can be translated into an efficient filterbank implementation using the scaling and wavelet filters. Figure 4 shows one iteration of the wavelet decomposition from both the point of view of the continuous domain and the discrete domain. To have the operator-like behavior on the input signal, one should put the operator wavelet as the wavelet $\tilde{\psi}$ at the analysis side, and its dual at the synthesis side. In that case, the filters of Fig. 4 are

$$\begin{aligned}
\tilde{G}_0(z) &= H(z), \\
G_0(z) &= H(z)\frac{A(z)}{A(z^2)}, \\
\tilde{G}_1(z) &= z^{-1}2^\alpha \frac{H(-z^{-1})}{A(z)}, \\
G_1(z) &= z^{-1}2^{-\alpha}H(-z^{-1})\frac{A(z)A(-z)}{A(z^2)}.
\end{aligned}$$

To correctly perform a wavelet decomposition of a signal $f(x)$, specified by its measurements $f(n)$ at the initial scale, one should apply a prefilter to obtain the coefficients $c_{(0)}[n]$ for its representation in $\mathcal{V}_0$. Here, we use the interpolation presentation of the B-spline representation at the initial scale.

In practice, we implement the operator wavelet transform using an FFT-based algorithm [39]. Given the analytical knowledge of all filters in the Fourier domain, this implementation method allows perfect reconstruction irrespective of the filter support that may be finite of infinite. It should be noted that using the FFT should be seen as a computational method that allow us to deploy a fast and exact algorithm within the constraints of periodic boundary conditions.

D. Decomposition of Elementary Singularities

Proposition 2 (Analytical Wavelet Footprint): Analyzing an elementary singularity associated to the fractional derivative (order γ_0, phase parameter τ_0, and located at position x_0) by the operator wavelet ψ (order γ, phase parameter τ) at scale i and position k leaves a footprint that can be approximated by the analytical form $2^{i(\gamma_0-1/2)}g(x_0/2^i - k; \gamma, \tau, \gamma_0, \tau_0)$, as defined by (24).

Proof: Given the properties of the operator wavelets and its fractional integrals, we can easily derive any wavelet coefficient $d_i[k]$ at scale i and position k of the discrete operator-wavelet decomposition for the given singularity:

$$\begin{aligned}
d_{(i)}[k] &= \left\langle \sqrt{2^{-i}}\,\psi(\cdot/2^i - k), \rho_{\tau_0}^{\gamma_0}(\cdot - x_0) \right\rangle \\
&= \sqrt{2^{-i}} \left\langle \left\{\overline{\partial}_{-\tau}^{\gamma}\phi\right\}(\cdot/2^i - k), \rho_{\tau_0}^{\gamma_0}(\cdot - x_0) \right\rangle \\
&= 2^{i(\gamma_0-1/2)} \left\langle \left\{\overline{\partial}_{\tau-\tau_0}^{\gamma-\gamma_0}\phi\right\}(\cdot/2^i - k), \partial_{\tau_0}^{\gamma_0}\rho_{\tau_0}^{\gamma_0}(\cdot - x_0) \right\rangle \\
&= 2^{i(\gamma_0-1/2)} \left\langle \left\{\overline{\partial}_{-\tau_0}^{-\gamma_0}\psi\right\}(\cdot/2^i - k), \partial(\cdot - x_0) \right\rangle \\
&= 2^{i(\gamma_0-1/2)} \underbrace{\left\{\overline{\partial}_{-\tau_0}^{-\gamma_0}\psi\right\}(x_0/2^i - k)}_{\longrightarrow g(x_0/2^i - k; \gamma, \tau, \gamma_0, \tau_0)}
\end{aligned}$$

∎

We first illustrate the analytical wavelet footprint by the non-sampled form $g(x; \gamma, \tau, \gamma_0, \tau_0)$. In Fig. 5, the singularities of Fig. 1 are analyzed by the operator wavelet ($\gamma = 3$, $\tau = 0$). Interestingly, changing the phase of the singularity influences the shape and symmetry of the operator wavelet, while changing the order of the singularity affects mainly the amplitude.

Proposition 3 (Lipschitz regularity): The signal model of (8) with singularities of order γ_k, $k = 1, \ldots, M$, is uniformly Lipschitz $\alpha_0 = \max_m(\gamma_m - 1)$. Consequently, there exists $A > 0$ such that the coefficients $d_{(i)}[k]$ at level i and position k of the operator wavelet decomposition of f satisfy

$$|d_{(i)}[k]| \leq As^{\alpha_0+1/2}, \quad (26)$$

where $s = 2^i$ is the scale.

Proof: Let us introduce $\alpha_m = \gamma_m - 1$ as the Lipschitz exponent of the m-th singularity, and the upperbound

$$A_m = \max_x |g(x; \gamma, \tau, \gamma_m, \tau_m)|$$

for the limiting form of the analytical wavelet footprint. Then, using scale $s = 2^i$, we can easily derive that

$$\begin{aligned}
|d_{(i)}[k]| &\approx \left| \sum_{m=1}^{M} a_m 2^{i(\gamma_m-1/2)} g(x_m/2^i - k; \gamma, \tau, \gamma_m, \tau_m) \right| \\
&\leq \sum_{m=1}^{M} s^{\alpha_m+1/2} |a_m| \underbrace{|g(x_m/s - k; \gamma, \tau, \gamma_m, \tau_m)|}_{\leq A_m} \\
&\leq As^{\alpha_0+1/2},
\end{aligned}$$

where $\alpha_0 = \max_m \alpha_m$ and $A = M \max_m(|a_m| A_m)$. ∎

When the operator wavelet (or its fractional integral) is used as a wavelet basis, the wavelet coefficients will be sampled versions of the continuous function. A useful feature is the mono- or bimodal character of these coefficients, as can be observed from Fig. 6. This property follows from the fact that the smoothing kernel—the interpolating B-spline—converges rapidly to the sinc-function [40]. Consequently, the smoothing
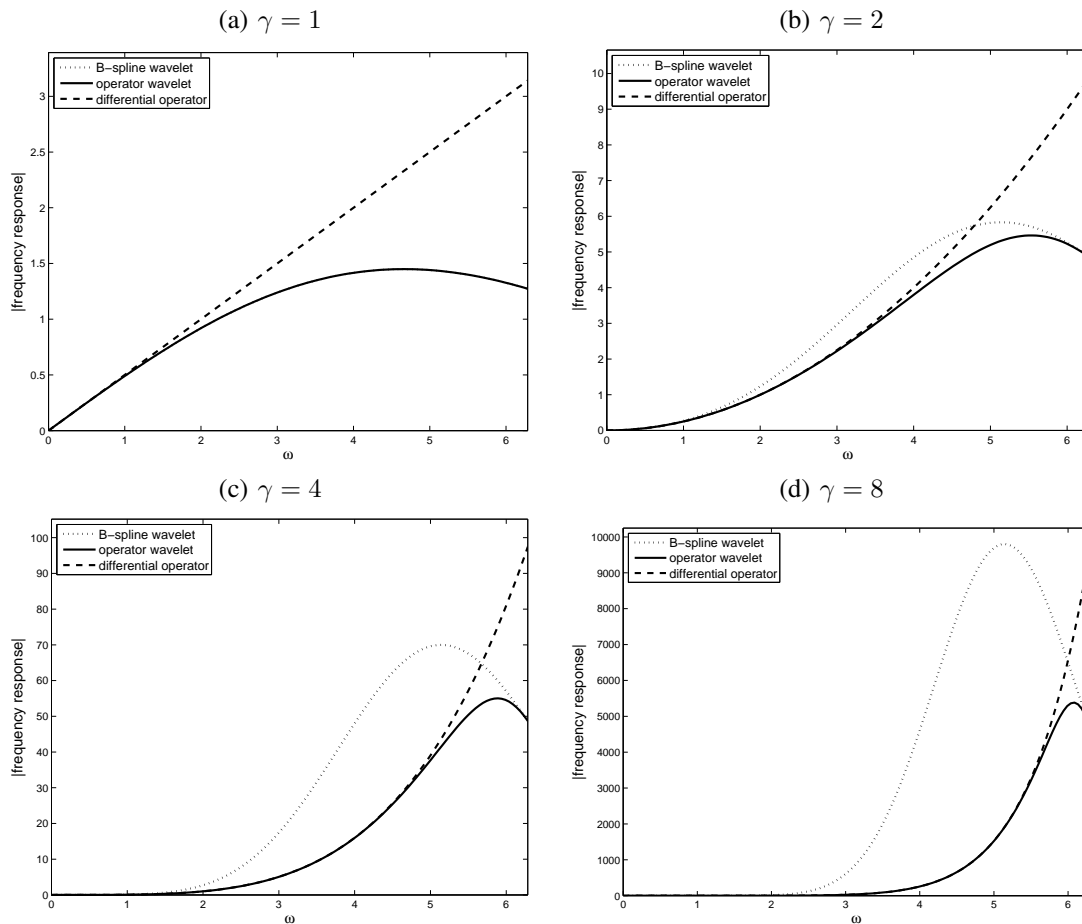
(a) $\gamma = 1$

(b) $\gamma = 2$

(c) $\gamma = 4$

(d) $\gamma = 8$

Fig. 2. Associated to the operator ∂_τ^γ, modulus of the frequency response of the (rescaled) B-spline wavelet, the operator wavelet, and the derivative operator, for various values of γ.

kernel at scale 0 will have a bandwidth of approximately $[-2\pi, 2\pi]$. Samples of this function at positions $k \in \mathbb{Z}$ all have the same sign, while samples of its derivatives could be mono- or bimodal only. This property is useful for applications, since the analytical wavelet footprint will have two local extrema at most.

IV. RESULTS AND DISCUSSION

We now illustrate the analytical footprints for the task of retrieving elementary singularities from an operator-wavelet decomposition. The algorithm that we are using is greedy and matches footprints one-by-one in a multiscale fashion; it is summarized in App. D.

A. Stepwise Parametric Fitting with Analytical Footprints

To illustrate the concept, we applied the algorithm to a piecewise polynomial signal of length 512 where the singularities are discontinuities; i.e., 8 singularities of the type $\rho_{0.5}^1$. We select the operator wavelet decomposition with parameters $\gamma = 8$, $\tau = 0$. In Fig. 7 (a), the decomposition of the signal on the operator wavelet basis is shown with 3 decomposition levels. The bimodal property allows us to find potential singularity locations by looking for the local extrema p_m at a given scale i', which are used as initial estimates

$2^{i'} p_m$ for the positions of the analytical footprints. Next, we perform parametric fitting of the expression of Proposition 2 using the Levenberg-Marquardt algorithm (Matlab 7.8.0) to solve the non-linear least-squares fitting criterion based on information at all scales. Both parameters, amplitude and edge position, are defined continuously. We use multiple initial estimates for the position (i.e., $2^{i'}(p_m - 1), \ldots, 2^{i'}(p_m + 1)$) and retain the parameters of the best fit. In Fig. 7 (c), we show the measured and fitted coefficients for the largest local extremum of the first decomposition level (corresponding the edge at position 305 in the signal). The fitted coefficients are then subtracted from the wavelet decomposition and the procedure is repeated for the next local extremum. In this way, we obtain a list of singularities that allows us to synthetize the singularity signal shown in Fig. 7 (b), together with is wavelet decomposition. The wavelet subbands are identical to those of the original signal (as they should be), while the lowpass subband contains the residual that encodes the smooth polynomial part. To compensate for the asymptotic nature of the analytical footprint, we adjust the amplitudes of the singularities by a global scaling factor obtained by linear regression between coefficients of all wavelets subbands of the synthetized singular signal and the ones of the original signal. Finally, by reconstructing the difference between the original lowpass and the one of the singularity signal, we obtain the
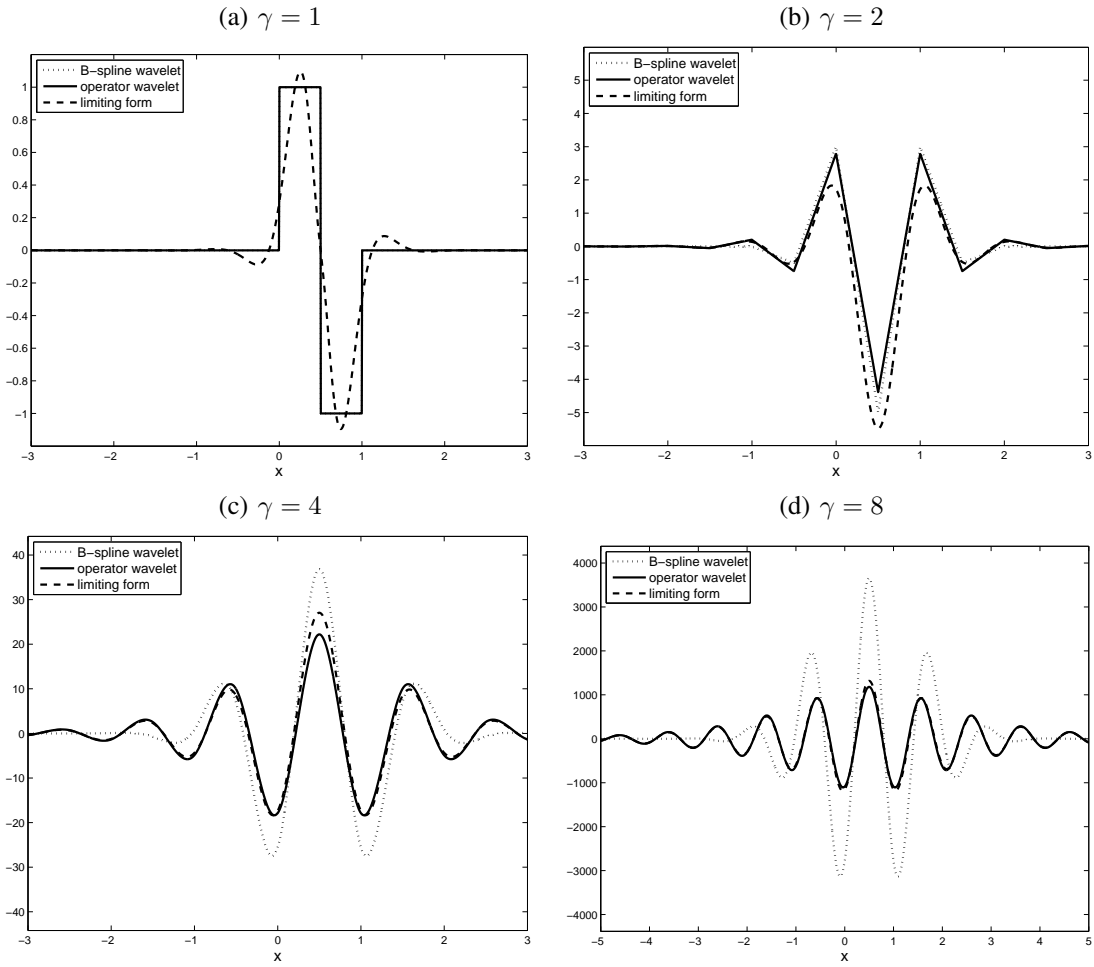
(a) $\gamma = 1$

(b) $\gamma = 2$

(c) $\gamma = 4$

(d) $\gamma = 8$

Fig. 3. The (rescaled) B-spline wavelet, the operator wavelet, and the limiting form, for various values of γ associated to the operator ∂_τ^γ, with $\tau = \gamma/2$.
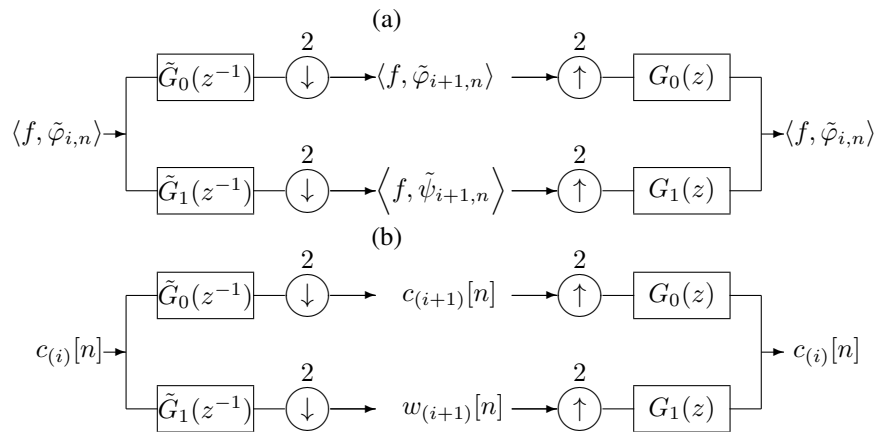
Fig. 4. The discrete wavelet transform for one decomposition level. (a) The continuous-domain representation. (b) The discrete-domain representation.
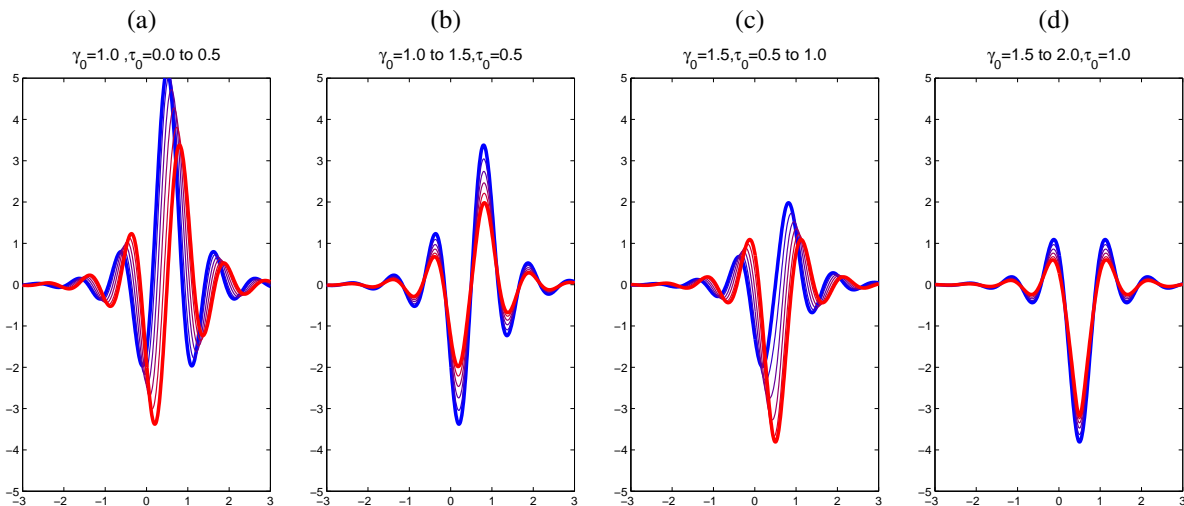
(a) $\gamma_0=1.0$, $\tau_0=0.0$ to 0.5 (b) $\gamma_0=1.0$ to 1.5, $\tau_0=0.5$ (c) $\gamma_0=1.5$, $\tau_0=0.5$ to 1.0 (d) $\gamma_0=1.5$ to 2.0, $\tau_0=1.0$

Fig. 5. Effect of the elementary singularity $\partial_{-\tau_0}^{-\gamma_0}$ on the operator wavelet ($\gamma = 3$, $\tau = 0$). Several subsets of singularities are shown in (a)-(d). The sweep-through starts in blue and ends in red.
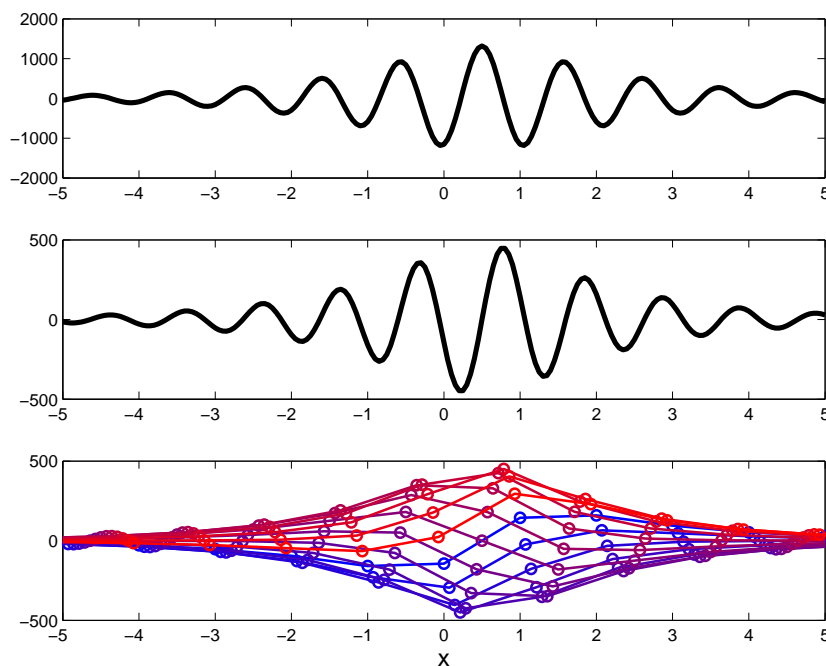

Fig. 6. Mono- or bimodal character of the wavelet coefficients of an edge singularity $\rho_{0.5}^1(x - x_0)$, where x_0 varies between 0 and 1 and 14 steps. Top: Operator wavelet $\gamma = 8$, $\tau = 0$. Middle: Operator wavelet acting on edge singularity. Bottom: Wavelet coefficients of the edge singularity at different shifts x_0 (red to blue) are sampled versions of the middle plot; they are all mono- or bimodal.

smooth part that can be added to the singularity signal and constitutes the reconstructed signal, see Fig. 7 (d). We show an example for another type of singularity (discontinuity of the derivative; i.e., $\gamma_0 = 2$, $\tau_0 = 1$) in Fig. 8.

One important issue is how well singularities can be separated when they are close to each other. For the proposed algorithm, singularities are fitted independently, and consequently their footprints can interfere if too close. We define the constant L as the distance over which the envelope of the operator wavelet is below a given percentage p of its peak value; given the sinc-like behavior of the smoothing kernel, this happens approximately for $L = (2p)^{-1}$ (see also Fig. 6 bottom). Therefore, avoiding interaction between footprints for

J decomposition levels requires singularities to be spaced at least $L \cdot 2^J$ samples apart. Notice that this condition is very similar to the one in [15], where the size of the wavelet filter played a central role. Empirically, we found that our one-by-one fitting procedure gave correct results for $p < 16\%$ in the noiseless case, corresponding to $L > 3$, which leads to a minimal signal separation of $3 \cdot 2^J$ for a decomposition with J levels.

Finally, we mention that artificial discontinuities may arise due to the periodic boundary conditions of our FFT-based implementation. To avoid this type of artifact, we linearly detrended the singularity signal before obtaining its decomposition and then added it back to the reconstructed low-pass
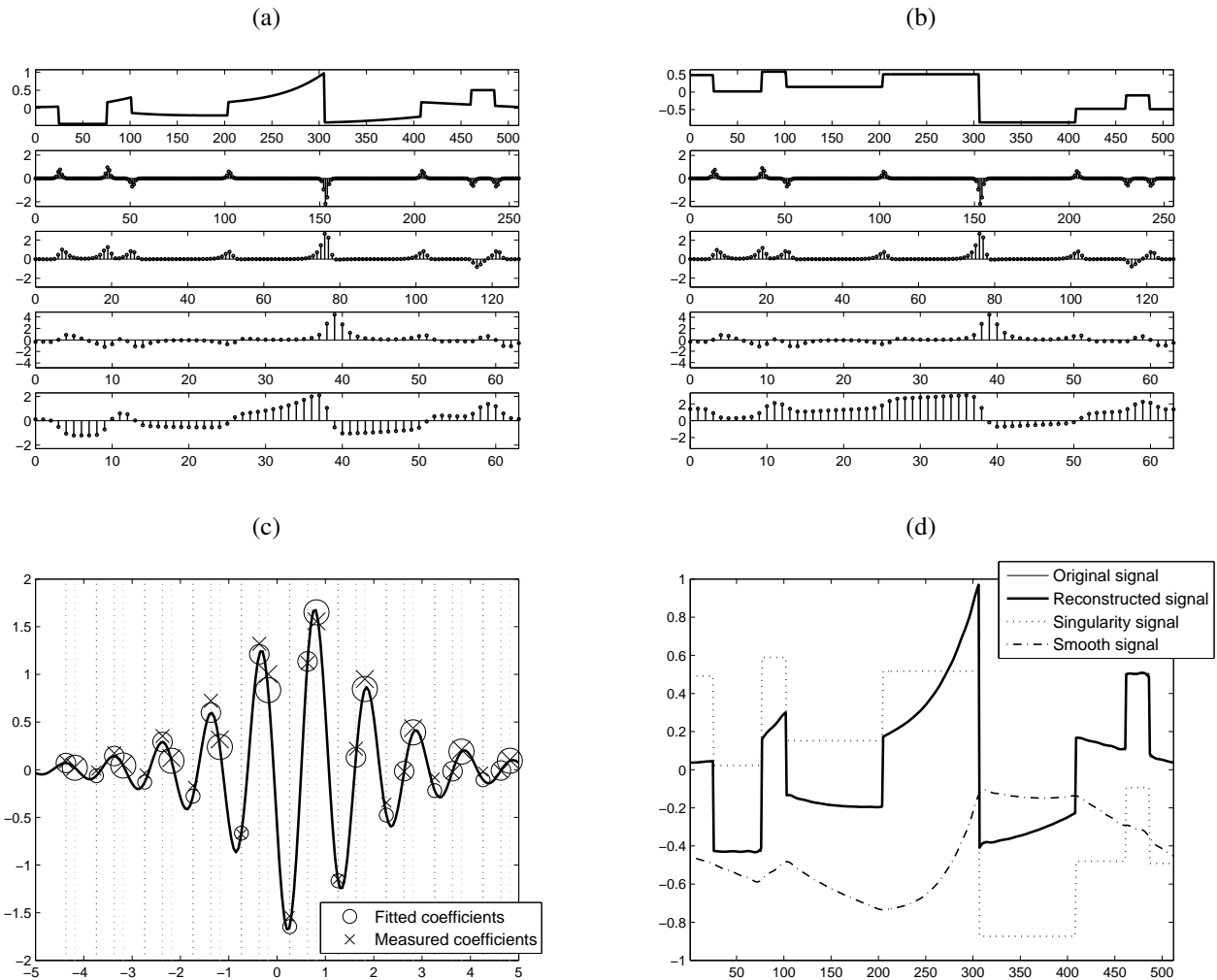
(a)

(b)

(c)

(d)

Fig. 7. (a) Original signal ($\gamma_0 = 1$, $\tau_0 = 1/2$) with its operator wavelet decomposition. (b) Singularity signal obtained from (a) with its operator wavelet decomposition. The wavelets coefficients in (a) and (b) are almost completely identical, while the difference in the lowpass subband encodes the smooth part. (c) Result of the fitting procedure for the large edge of the signal at position 305. The fitting uses all scales at the same time; coefficients from coarses scales are larger. (d) Reconstructed signal, together with the constituting singularity and smooth signal parts. The SNR of the reconstruction is 43dB.

residual.

Although our algorithm is not specifically designed for denoising, it can yield competitive results for the class of singular signals satisfying (8). In Fig. 9, we show the outcome when applying the same algorithm as before to the signal deteriorated with additive Gaussian noise (SNR 20dB). All signal discontinuities are well recovered and the remaining noise originates from the residual lowpass subband; the total SNR improvement is about 7dB.

B. Discussion

We demonstrated that it is possible to extract and characterize singularities from the operator-wavelet decomposition using the analytical wavelet footprints. The analytical form replaces an explicit dictionary that needs to be learned and that suffers from redundancy in the case of shift-variant wavelet signatures (as occur with non-redundant bases). The algorithm is related to matching pursuit [41] in the sense that the singularities are fitted one by one. However, the dictionary

is never explicit and the parameters (a_m, x_m) are retrieved by a numerical optimization algorithm. Discretizing the positions x_m on the (uniform) measurement grid would allow to solve the problem with matching pursuit or sparsity-pursuing algorithms [3]. While applying algorithms from the discrete setting is outside the scope of this paper, theoretical results on the exact recovery criterion can shed light on the minimum spacing between singularities [42], [43]. Specifically, for the case of spike deconvolution with Morlet wavelet and small noise, the minimum spacing of $5 \cdot \tilde{s}$ was found, with $\tilde{s}$ the width (standard deviation) of the Gaussian smoothing kernel [3], [44]. For the operator wavelet, we have $\tilde{s} \approx 2^{J+1}$, which makes the bound $10 \cdot 2^J$. Empirically, we found a lower bound of $3 \cdot 2^J$ in the noiseless case, which is the same order of magnitude; the difference could be explained by high order of the operator wavelet that we use ($\gamma = 8$) and the fact that we exploit the knowledge that only two singularities needs to be fitted. Another advantage of parametric fitting of the analytical footprints is the ability to reach subsample resolution since the
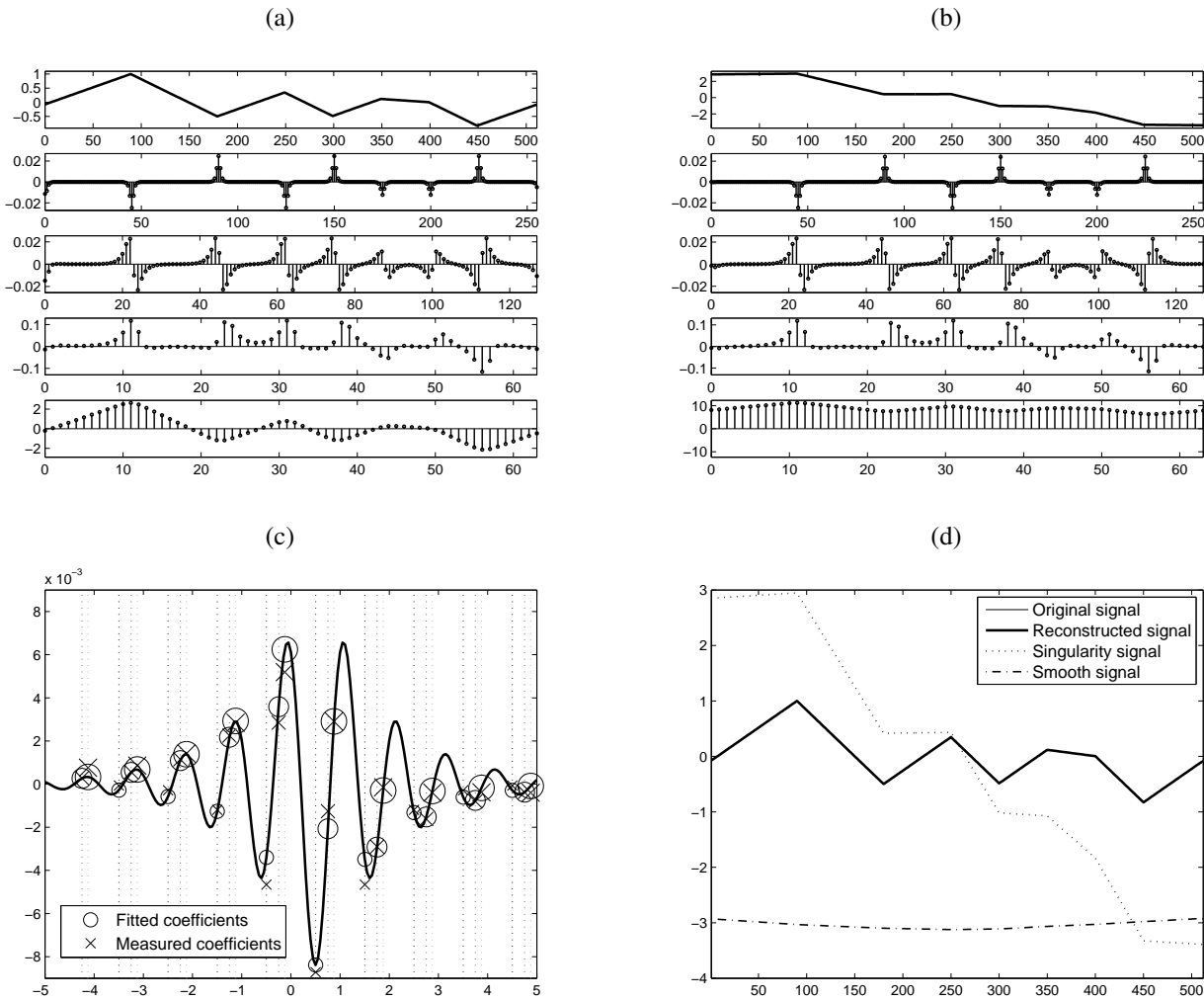
(a)

(b)

(c)

(d)

Fig. 8. (a) Original signal ($\gamma_0 = 2$, $\tau_0 = 1$) with its operator wavelet decomposition. (b) Singularity signal obtained from (a) with its operator wavelet decomposition. The wavelets coefficients in (a) and (b) are almost completely identical, while the difference in the lowpass subband encodes the smooth part. (c) Result of the fitting procedure for the large edge of the signal at position 90. The fitting uses all scales at the same time; coefficients from coarse scales are larger. (d) Reconstructed signal, together with the constituting singularity and smooth signal parts. The SNR of the reconstruction is 62dB.
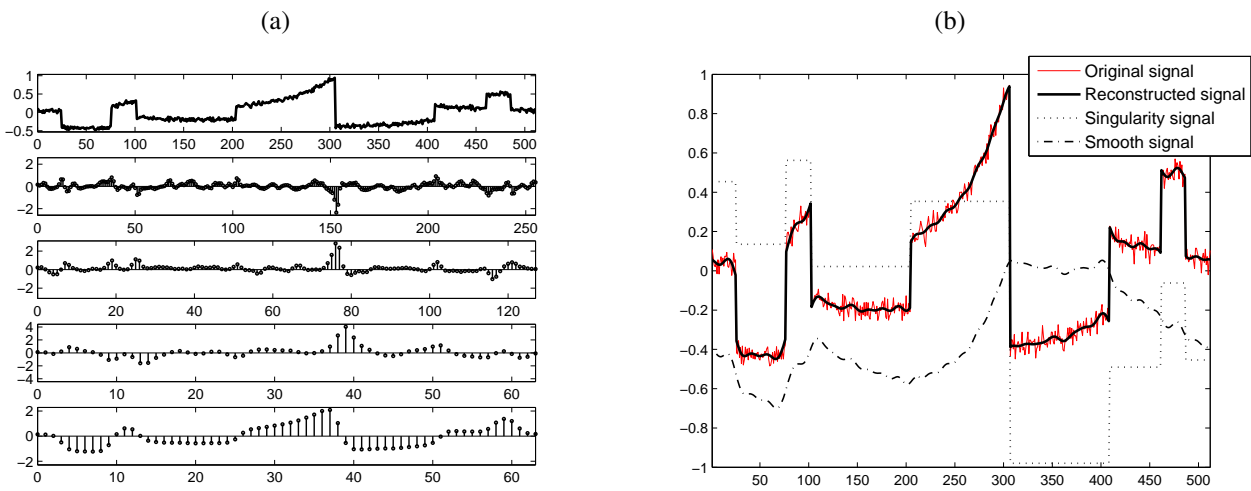
(a)

(b)

Fig. 9. The SNR improvement of the reconstructed signal is 7dB (noisy signal 20dB).

problem is completely formulated in the continuous domain; this opens the door to superresolution. The stepwise fitting algorithm that was applied in Sect. IV-A is primarily meant as a proof-of-concept. We believe that it may be improved on several counts.

In the present implementation, the singularities are fitted one after the other. A more evolved version could fit multiple singularities at the same time, explicitly taking into account their interference patterns. Another option is to rely on additional information provided by different operator wavelets. One attractive choice is to use a Hilbert-pair of operator wavelets [45], [46]; i.e., the ones corresponding to order γ with phase parameter τ, and order γ with phase parameter $\tau + 1/2$, respectively.

We should also mention that the approach is not necessarily optimal for denoising. Although the operator wavelet decomposition is a semi-orthogonal one, that is, wavelets of different scales are orthogonal but not within the same scale. Therefore, white noise will become correlated between wavelet coefficients at the same scale. The fitting procedure could be extended to take into account the correlation. Also, depending on the amount of noise, the local extrema could be detected at a different decomposition level or using a more robust detector. Moreover, the number of decomposition levels directly influences the amount of smoothing in the lowpass subband.

Finally, we mention that the proposed algorithm preselects the type of singularity that will be fitted. Although the same operator-wavelet decomposition can be used to deal with different singularities, going beyond this limitation is a remaining challenge for future research. Our attempts to let the parametric fitting also take care of the order or the phase of the singularities did not give satisfactory results. Another problem related to mixing signatures of singularities of different order is their significant difference in dynamic range (e.g., compare Figs. 7 (a) and 8 (a)).

V. Conclusion

In this paper, we proposed a particular wavelet basis, named operator wavelets, that is part of the family of fractional B-spline wavelets. The corresponding (non-redundant) wavelet transform acts as a multiscale fractional derivative operator, which have been studied extensively in mathematics. We provided a closed-form formula for the response of these wavelets to the whole class of self-similar (γ, τ) singularities. We also showed a practical algorithm to extract the singularities from a given signal and separate and reconstruct the singularity and the smooth parts. One attractive feature of our approach approach is that it works for non-redundant decompositions and explicitly takes into account the effect of subsampling. This could open new possibilities for signal analysis on compact decompositions.

Appendix A
Construction of Fractional B-spline Wavelets

These B-splines satisfy the three admissibility conditions for a scaling function [17], [18]:

(i) They generate a Riesz basis; i.e., the autocorrelation filter is bounded by two constants $0 < C_0 \leq \left| A(e^{j\omega}) \right| \leq C_1 < \infty$.

(ii) They fulfill the partition of unity:

$$\sum_n \beta_\tau^\alpha(x - n) = 1. \tag{27}$$

(iii) They satisfy a two-scale relation.

Consequently, the B-splines generate a multi-resolution analysis of $L_2(\mathbb{R})$; that is, a sequence of nested subspaces

$$\cdots \subset \mathcal{V}_2 \subset \mathcal{V}_1 \subset \mathcal{V}_0 \subset \mathcal{V}_{-1} \subset \mathcal{V}_{-2} \subset \cdots \subset L_2(\mathbb{R}). \tag{28}$$

We now revisit and extend the design strategy for the semi-orthogonal spline wavelet transform that was initially proposed in [31]. To that end, we select the wavelet space

$$\mathcal{W}_i = \text{span}_{n \in \mathbb{Z}} \left\{ \sqrt{2^{-i}} \psi \left(\frac{x}{2^i} - n \right) \right\} \tag{29}$$

as the orthogonal complement of $\mathcal{V}_i$, such that $\mathcal{V}_i \oplus \mathcal{W}_i = \mathcal{V}_{i-1}$. The wavelet is therefore constrained to be orthogonal to all integer-shifted versions of the scaling function at the same scale, which also implies orthogonality to wavelets at different scales; i.e., $\mathcal{W}_i \perp \mathcal{W}_j$, for $i \neq j$.

By construction, the wavelet at scale 1 is included in $\mathcal{V}_0$, which is expressed as

$$\psi \left(\frac{x}{2} \right) = \sqrt{2} \sum_k w[k] \beta_\tau^\alpha(x - k). \tag{30}$$

It also has to fulfill the orthogonality condition $\mathcal{V}_1 \perp \mathcal{W}_1$:

$$\left\langle \psi \left(\frac{\cdot}{2} \right), \beta_\tau^\alpha \left(\frac{\cdot}{2} - n \right) \right\rangle = 0, \quad n \in \mathbb{Z}. \tag{31}$$

Taking the z-transform of (31) results into

$$W(z)H(z^{-1})A(z) + W(-z)H(-z^{-1})A(-z) = 0. \tag{32}$$

This condition requires $W(z)H(z^{-1})A(z)$ to be an odd polynomial; thus the degree of freedom of $Q(z^2)$.

Appendix B
Proof of Proposition 1

First, we verify that the proposed form of $W(z)$ satisfies the semi-orthogonality condition of (32). We then derive the Riesz bounds of the wavelet filter as

$$
\begin{aligned}
R(e^{j\omega}) &= \sum_k \left| \hat{\psi}(\omega + 2\pi k) \right|^2 \\
&= \frac{1}{2} \left| W(z^{1/2}) \right|^2 A(z^{1/2}) + \frac{1}{2} \left| W(-z^{1/2}) \right|^2 A(-z^{1/2}) \\
&= \left| Q(z) \right|^2 A(z^{1/2}) A(-z^{1/2}) \\
&\quad \left(\frac{\left| H(-z^{-1/2}) \right|^2}{2} A(-z^{1/2}) + \frac{\left| H(z^{1/2}) \right|^2}{2} A(z^{1/2}) \right) \\
&= \left| Q(z) \right|^2 A(z^{1/2}) A(-z^{1/2}) A(z).
\end{aligned}
$$

Consequently, the wavelet generates a Riesz basis if $0 < C_0 \leq \left| Q(e^{j\omega}) \right| \leq C_1 < \infty$. This guarantees a stable perfect reconstruction filterbank when implementing the discrete wavelet transform.

To characterize the operator-like behavior of the semi-orthogonal spline wavelet, we rewrite (18) as

$$
\begin{aligned}
2\hat{\psi}(2\omega) &= \sqrt{2}W(e^{j\omega})\hat{\beta}_\tau^\alpha(\omega) \\
&= \sqrt{2}e^{-j\omega}Q(e^{j2\omega})H(-e^{-j\omega})A(-e^{j\omega}) \cdot \frac{\hat{\Delta}_\tau^\gamma(e^{j\omega})}{\hat{\partial}_\tau^\gamma(\omega)} \\
&= \hat{\partial}_\tau^\gamma(-\omega)\sqrt{2}e^{-j\omega} \\
&\quad \frac{Q(e^{j2\omega})H(-e^{-j\omega})A(-e^{j\omega})}{\hat{\Delta}_\tau^\gamma(e^{-j\omega})}\frac{\hat{\Delta}_0^{2\gamma}(e^{j\omega})}{\hat{\partial}_0^{2\gamma}(\omega)} \qquad (33) \\
&= \hat{\partial}_\tau^\gamma(-\omega)2^{-\alpha}e^{-j\omega}Q(e^{j2\omega})A(-e^{j\omega})\hat{\beta}_0^{2\gamma-1}(\omega) \qquad (34)
\end{aligned}
$$

where we have used the identity $H(-z) = 2^{-\alpha-\frac{1}{2}}\hat{\Delta}_\tau^{\alpha+1}(z)$. Note that in (34), none of the factors except $\hat{\partial}_\tau^\gamma(-\omega)$ cancels at $\omega = 0$. Therefore, we derive the asymptotic form of (34) as

$$
\mathcal{F}\{\psi(\cdot/2)\}(\omega) = C_2 e^{-j\omega}\hat{\partial}_\tau^\gamma(-\omega) + O(|\omega|^{\gamma+1}), \quad \text{as } \omega \to 0, \tag{35}
$$

with the constant $C_2 = \lim_{\omega\to0} 2^{-\alpha}Q(e^{j2\omega})A(-e^{j\omega}) = \frac{2^{-\gamma+2}}{\pi^{2\gamma}}\zeta(2\gamma)(2^{2\gamma}-1)Q(1)$, where $\zeta(s) = \sum_{n>0}\frac{1}{n^s}$ is the Riemann zeta function. ∎

APPENDIX C
PROOF OF PROPOSITION 1

First, we show that the operator wavelet of (22) is obtained for $Q(z^2) = 2^\alpha/(A(z)A(-z))$, which is bounded and thus a valid choice. For this $Q(z^2)$, we find in the Fourier domain that

$$
2\hat{\psi}(2\omega) = \hat{\partial}_\tau^\gamma(-\omega)e^{-j\omega}\frac{\hat{\beta}_0^{2\gamma-1}(\omega)}{A(e^{j\omega})}. \tag{36}
$$

The term $1/A(e^{j\omega})$ can be recognized as the interpolation prefilter of the 2γ-th order symmetric B-spline. By identifying the interpolating B-spline $\beta_{\text{int}}^{2\gamma-1}$, we further develop (36) as

$$
2\hat{\psi}(2\omega) = \hat{\partial}_\tau^\gamma(-\omega)e^{-j\omega}\hat{\beta}_{\text{int}}^{2\gamma-1}(\omega), \tag{37}
$$

which corresponds in the spatial domain to

$$
\psi\left(\frac{x}{2}\right) = \overline{\partial}_\tau^\gamma\beta_{\text{int}}^{2\gamma-1}(x-1). \tag{38}
$$

The resulting wavelet filter becomes

$$
W(z) = z^{-1}2^\alpha\frac{H(-z^{-1})}{A(z)}, \tag{39}
$$

which can be rewritten as

$$
W(z)\frac{1}{\hat{\Delta}_\tau^\gamma(z^{-1})}A(z) = z^{-1}, \tag{40}
$$

and thus satisfies the wavelet filter condition derived in App. A.

Second, the expression of the operator wavelet (36) can be further manipulated in the Fourier domain:

$$
2\hat{\psi}(2\omega) = \hat{\partial}_\tau^\gamma(-\omega)\frac{e^{-j\omega}}{1+|\omega|^{2\gamma}\sum_{k\neq0}\frac{1}{|\omega+2\pi k|^{2\gamma}}}. \tag{41}
$$

The proposed wavelet depends on the space defined by the B-spline scaling function, but is independent of the choice of a particular spline scaling function. Since the second factor in (41) is essentially constant for $\omega \leq \pi$, we may infer that

this wavelet closely matches the frequency response of the operator over a large range in the Fourier domain. Indeed, the order of the second term of the Taylor development at $\omega = 0$ increased from $\gamma + 1$ to 3γ:

$$
\hat{\psi}(\omega) \propto \hat{\partial}_\tau^\gamma(-\omega/2)e^{-j\omega/2} + O(|\omega|^{3\gamma}), \quad \text{as } \omega \to 0. \tag{42}
$$

Finally, we derive an explicit form of $\partial_{-\tau_0}^{-\gamma_0}\psi$. We start from (41) and use the fact that the wavelet $\hat{\psi}(2\omega)$ has most of its energy mostly around π and $-\pi$. This allows us to approximate the sum in the denominator by two dominant terms

$$
\begin{aligned}
&\frac{2\hat{\psi}(2\omega)}{(-j\omega)^{\gamma_0/2-\tau_0}(j\omega)^{\gamma_0/2+\tau_0}} \\
&\approx \frac{e^{-j\omega}(j\omega)^{(\gamma-\gamma_0)/2-(\tau+\tau_0)}(-j\omega)^{(\gamma-\gamma_0)/2+(\tau+\tau_0)}}{1+\left|\frac{\omega}{\omega-2\pi}\right|^{2\gamma}+\left|\frac{\omega}{\omega+2\pi}\right|^{2\gamma}}.
\end{aligned}
$$

We now focus on the positive frequencies $\omega > 0$ and apply the change of variables $\omega = \pi(1+\eta)$ where η is close to 0:

$$
\begin{aligned}
&\hat{\partial}_{-\tau_0}^{-\gamma_0}2\hat{\psi}^+(2\omega) \\
&= \frac{e^{-j\pi(1+\eta)}\pi^{\gamma-\gamma_0}(-j(1+\eta))^{\frac{\gamma-\gamma_0}{2}-\tau-\tau_0}(j(1+\eta))^{\frac{\gamma-\gamma_0}{2}+\tau+\tau_0}}{1+\left|\frac{1+\eta}{1-\eta}\right|^{2\gamma}+\left|\frac{1+\eta}{3+\eta}\right|^{2\gamma}} \\
&\approx \frac{e^{-j\pi(1+\eta)}\pi^{\gamma-\gamma_0}e^{-j\pi(\tau+\tau_0)}(1+\eta)^{\gamma-\gamma_0}}{1+\left|\frac{1+\eta}{1-\eta}\right|^{2\gamma}} \\
&\approx \frac{e^{-j\pi(1+\eta)}\pi^{\gamma-\gamma_0}e^{-j\pi(\tau+\tau_0)}e^{(\gamma-\gamma_0)\eta}}{1+e^{4\gamma\eta}},
\end{aligned}
$$

where the last step makes use of the approximation $1+\eta \approx e^\eta$. This latter expression we then use to compute the Fourier inverse of the analytical signal of the wavelet:

$$
\begin{aligned}
&\partial_{-\tau_0}^{-\gamma_0}\psi^+(x) \\
&= \frac{1}{2\pi}\int_{-\infty}^{+\infty}\hat{\partial}_{-\tau_0}^{-\gamma_0}\hat{\psi}^+(\omega)e^{j\omega x}d\omega \\
&= \frac{1}{\pi}\int_{-\infty}^{+\infty}\hat{\partial}_{-\tau_0}^{-\gamma_0}\hat{\psi}^+(2\omega)e^{j2\omega x}d\omega \\
&\approx -\frac{\pi^{\gamma-\gamma_0}e^{-j\pi(\tau+\tau_0)}}{2}\int_{-\infty}^{+\infty}\frac{e^{(\gamma-\gamma_0)\eta}}{1+e^{4\gamma\eta}}e^{j\pi(2x-1)(1+\eta)}d\eta \\
&= -\frac{\pi^{\gamma-\gamma_0}e^{-j\pi(\tau+\tau_0-2x)}}{8\gamma} \\
&\quad \underbrace{\int_0^1\xi^{-\frac{\gamma-\gamma_0}{4\gamma}-j\frac{\pi(2x-1)}{4\gamma}}(1-\xi)^{-1+\frac{\gamma-\gamma_0}{4\gamma}+j\frac{\pi(2x-1)}{4\gamma}}d\xi}_{B\left(1-\frac{\gamma-\gamma_0}{4\gamma}-j\frac{\pi(2x-1)}{4\gamma},\frac{\gamma-\gamma_0}{4\gamma}+j\frac{\pi(2x-1)}{4\gamma}\right)} \\
&= -\frac{\pi^{\gamma-\gamma_0+1}e^{j\pi(2x-(\tau+\tau_0))}}{8\gamma\sin\left(\frac{\pi(\gamma-\gamma_0)}{4\gamma}+j\frac{\pi^2(2x-1)}{4\gamma}\right)}
\end{aligned}
$$

where we used the change of variables $1/(1+e^{4\gamma\eta}) = \xi$ to identify the Beta function for which the identity $B(1-a,a) = \Gamma(1-a)\Gamma(a) = \pi/\sin(a\pi)$ holds. This ultimately yields the following asymptotic expression for the operator wavelet and

its fractional integrals:

$$\partial_{-\tau_0}^{-\gamma_0}\psi(x) \approx -\frac{\pi^{\gamma-\gamma_0+1}}{4\gamma}\text{Re}\left[\frac{e^{j\pi(2x-(\tau+\tau_0))}}{\sin\left(\frac{\pi(\gamma-\gamma_0)}{4\gamma}+j\frac{\pi^2(2x-1)}{4\gamma}\right)}\right].$$
(43)

The complex argument of the sin-function can be evaluated using $\sin(a+jb) = \sin(a)\cosh(b)+j\cos(a)\sinh(b)$. ∎

APPENDIX D
ALGORITHM FOR STEPWISE PARAMETRIC FITTING

We first choose the operator wavelet transform (order γ, phase τ). Next, we select the singularity type that we want to recover (order $\gamma_0 < \gamma$, phase τ_0). The signal f is decomposed in the operator wavelet basis, resulting in coefficients $d_{(i)}[k]$ at scales $i = 1, \ldots, J+1$ and positions k. For a chosen subband at scale i', we now make a list of the local extrema p_m, $m = 1, \ldots, M$. The core of the algorithm will now fit singularities one by one for each local extremum. Specifically, we optimize the parameters of the analytical footprint (amplitude a_m, position x_m) using the Levenberg-Marquardt optimization algorithm based on the multiscale information of the wavelet coefficients $d_{(i)}[k]$, $i = 1, \ldots, J$. We try several initial estimates for the position $x_m : 2^{i'}(p_m - 1), \ldots, 2^{i'}(p_m + 1)$. Next, the fitted analytical footprint is subtracted from the coefficients $d_{(i)}[k]$ ($i = 1, \ldots, J$). After fitting M singularities, we synthetize the singularity signal f_1 using $a_m\rho_{\tau_0}^{\gamma_0}(x - x_m)$ and obtain its wavelet coefficients $d'_{(i)}[k]$. We now adjust the singularity amplitudes a_m by least-squares solution of the optimal scaling factor between $d'_{(i)}[k]$ and the initial coefficients $d_{(i)}[k]$. Finally, we reconstruct the smooth signal f_0 from the residual lowpass $c_{(J)}[k] - c'_{(J)}[k]$ only. Our approximation of f based on the singular signal model is given by $f_1 + f_0$.

REFERENCES

[1] S. Mallat, "A theory for multiresolution signal decomposition: The wavelet decomposition," *IEEE Trans. Pattern Anal. Mach. Intell.*, vol. 11, pp. 674–693, 1989.

[2] I. Daubechies, "The wavelet transform, time-frequency localization and signal analysis," *IEEE Transactions on Information Theory*, vol. 36, no. 5, pp. 961–1005, 1990.

[3] S. Mallat, *A Wavelet Tour of Signal Processing: The Sparse Way*, Academic Press, San Diego (CA), 2009.

[4] S. Mallat, "Zero-crossings of a wavelet transform," *IEEE Transactions on Information Theory*, vol. 37, no. 4, pp. 1019–1033, July 1991.

[5] S. Mallat and S. Zhong, "Characterization of signals from multiscale edges," *IEEE Transactions on Pattern Analysis and Machine Intelligence*, vol. 14, no. 7, pp. 710–732, July 1992.

[6] S. Mallat and W. L. Hwang, "Singularity detection and processing with wavelets," *IEEE Transactions on Information Theory*, vol. 38, pp. 617–643, 1992.

[7] Yu-Ping Wang, "Image representations using multiscale differential operators," *IEEE Transactions on Image Processing*, vol. 8, no. 12, pp. 1757–1771, 1999.

[8] J. F. Clearbout and F. Muir, "Robust modeling of erratic data," *Geophysics*, vol. 38, no. 5, pp. 826–844, 1973.

[9] F. Santosa and W. W. Symes, "Linear inversion of band-limited reflection seismograms," *SIAM J. Sci. Statist. Computing*, vol. 7, no. 4, pp. 1307–1330, 1986.

[10] F. J. Herrmann, "Singularity characterization by monoscale analysis: Application to seismic imaging," *Appl. Comput. Harmon. Anal.*, vol. 11, pp. 64–88, 2001.

[11] M. Maysami, *Lithology constraints from seismic waveforms: application to opal-A to opal-CT transition*, Ph.D. thesis, University of British Columbia, 2008.

[12] F. J. Herrmann, "Seismic deconvolution by atomic decomposition: a parametric approach with sparseness constraints," *Integr.*, vol. 12, no. 1, pp. 69–91, 2005.

[13] C. Li, C. Zheng, and C. Tai, "Detection of ECG characteristic points using wavelet transforms," *IEEE Transactions on Biomedical Engineering*, vol. 42, no. 1, pp. 21–28, 1995.

[14] Brian M. Sadler and Ananthram Swami, "Analysis of multiscale products for step detection and estimation," *IEEE Transactions on Information Theory*, vol. 45, no. 3, pp. 1043–1051, Apr. 1999.

[15] P. L. Dragotti and M. Vetterli, "Wavelet footprints: Theory, algorithms, and applications," *IEEE Transactions on Signal Processing*, vol. 51, pp. 1306–1323, 2003.

[16] V. Bruni and D. Vitulano, "Wavelet based signal denoising via simple singularities approximation," *Signal Processing*, vol. 86, pp. 859–876, 2006.

[17] M. Unser and T. Blu, "Fractional splines and wavelets," *SIAM Review*, vol. 42, pp. 43–67, 2000.

[18] T. Blu and M. Unser, "A complete family of scaling functions: The (α, τ)-fractional splines," in *Proceedings of the Twenty-Eighth IEEE International Conference on Acoustics, Speech, and Signal Processing (ICASSP'03)*, Hong Kong, Apr. 2003, IEEE.

[19] K. S. Miller and B. Ross, *An Introduction to the Fractional Calculus and Fractional Differential Equations*, John Wiley & Sons Inc., 1993.

[20] S. G. Samko, A. A. Kilbas, and O. I. Marichev, *Fractional Integrals and Derivative. Theory and Applications*, Gorden & Breach Sci. Publishers, 1993.

[21] I. Podlubny, *Fractional Differential Equaitons*, Academic Press, 1998.

[22] A. A. Kilbas, H. M. Srivastava, and J. J. Trujillo, *Theory and Applications of Fractional Differential Equations*, Saunders Ltd., 2006.

[23] F. Mainardi, *Fractional Calculus and Waves in Linear Viscoelasticity: An Introduction to Mathematical Models*, World Scientific Pub Co, 2010.

[24] R. Gorenflo and F. Mainardi, *Fractals and Fractional Calculus in Continuum Mechanics*, vol. 378 of *CISM Courses and Lectures*, chapter Fractional Calculus: Integral and Differential Equations of Fractional Order, pp. 223–276, Springer Verlag, 1997.

[25] M. D. Ortigueira, "On the fractional central differences and derivatives," *Journal of Vibration and Control*, vol. 14, no. 9–10, pp. 1255–1266, 2008.

[26] M. Unser and T. Blu, "Self-similarity: Part I—Splines and operators," *IEEE Transactions on Signal Processing*, vol. 55, no. 4, pp. 1352–1363, Apr. 2007.

[27] Israïl Moiseevich Gel'fand and Georgii Evgen'evich Shilov, *Properties and Operations*, vol. I of *Generalized Functions*, Academic Press, 1964, translated by Eugene Saletan.

[28] Laurent Schwartz, *Théorie des Distributions*, Hermann, 1998.

[29] D. C. Champeney, *A handbook of Fourier theorems*, Cambridge University Press, 1987.

[30] T. Blu and M. Unser, "Wavelets, fractals, and radial basis functions," *IEEE Transactions on Signal Processing*, vol. 50, no. 3, pp. 543–553, Mar. 2002.

[31] M. Unser, A. Aldroubi, and M. Eden, "A family of polynomial spline wavelet transforms," *Signal Processing*, vol. 30, pp. 141–162, 1993.

[32] G. Battle, "A block spin construction of ondelettes. Part I: Lemarié functions," *Commun. Math. Phys.*, vol. 110, pp. 601–615, 1987.

[33] Charles K. Chui and Jian-Zhong Wang, "A cardinal spline approach to wavelets," *Proceedings of the American Mathematical Society*, vol. 113, no. 3, pp. 785–793, Nov. 1991.

[34] Charles Micchelli, Christophe Rabut, and Florencia I. Utreras, "Using the refinement equation for the construction of pre-wavelets III: Elliptic splines," *Numerical Algorithms 1*, , no. 4, pp. 331–352, 1991.

[35] I. Khalidov, D. Van De Ville, T. Blu, and M. Unser, "Construction of wavelet bases that mimic the behaviour of some given operator," in *Proceedings of the SPIE Conference on Mathematical Imaging: Wavelet XII*, San Diego CA, USA, August 26-29, 2007, vol. 6701, pp. 67010S–1–67010S–7.

[36] D. Van De Ville and M. Unser, "Complex wavelet bases, steerability, and the Marr-like pyramid," *IEEE Transactions on Image Processing*, vol. 17, no. 11, pp. 2063–2080, November 2008.

[37] M. Unser, D. Sage, and D. Van De Ville, "Multiresolution monogenic signal analysis using the Riesz-Laplace wavelet transform," *IEEE Transactions on Image Processing*, vol. 18, no. 11, pp. 2402–2418, November 2009.

[38] M. Unser and D. Van De Ville, "Higher-order Riesz transforms and steerable wavelet frames," in *Proceedings of the 2009 IEEE International Conference on Image Processing (ICIP'09)*, Cairo, Egypt, November 7-11, 2009, pp. 3801–3804.

[39] T. Blu and M. Unser, "The fractional spline wavelet transform: Definition and implementation," in *Proceedings of the Twenty-Fifth IEEE International Conference on Acoustics, Speech, and Signal Processing (ICASSP'00)*, Istanbul, Turkey, June 5-9, 2000, vol. I, pp. 512–515.

[40] A. Aldroubi, M. Unser, and M. Eden, "Cardinal spline filters: Stability and convergence to the ideal sinc interpolator," *Signal Processing*, vol. 28, no. 2, pp. 127–138, August 1992.

[41] S. Mallat and Z. Zhang, "Matching pursuit with time-frequency dictionaries," *IEEE Transactions on Signal Processing*, vol. 41, pp. 3397–3415, 1993.

[42] J. A. Tropp, "Greed in good: algorithmic results for sparse approximation," *IEEE Transactions on Information Theory*, vol. 50, no. 10, pp. 2231–2242, 2004.

[43] R. Gribonval and M. Nielsen, "Beyond sparsity: Recovering structured representations by ℓ^1 minimization and greedy algorithms," *Adv. Comput. Math.*, vol. 28, no. 1, pp. 23–41, 2008.

[44] C. Dossal and S. Mallat, "Sparse spike deconvolution with minimum scale," in *Proceedings of SPARS05*, 2005.

[45] N. Kingsbury, "Complex wavelets for shift invariant analysis and filtering of signals," *Applied and Computational Harmonic Analysis*, vol. 10, no. 3, pp. 234–253, May 2001.

[46] K.N. Chaudhury and M. Unser, "Construction of Hilbert transform pairs of wavelet bases and Gabor-like transforms," *IEEE Transactions on Signal Processing*, vol. 57, no. 9, pp. 3411–3425, September 2009.

Dimitri Van De Ville (M'02) received the M.S. degree in engineering and computer sciences from Ghent University, Belgium, in 1998, as well as the Ph.D. degree, in 2002. He obtained a grant as Research Assistant with the Fund for Scientific Research Flanders Belgium (FWO). In 2002, he joined Prof. M. Unser's Biomedical Imaging Group at the École Polytechnique Fédérale de Lausanne (EPFL), Switzerland. In December 2005, he became responsible for the Signal Processing Unit at the University Hospital of Geneva, Switzerland, as part of the Centre d'Imagerie Biomédicale (CIBM). In 2009, he has been the recipient of a Swiss National Science Foundation professorship and currently holds a joint position at the University of Geneva and the EPFL. His research interests include wavelets, sparsity, pattern recognition, and their applications in biomedical imaging, such as functional magnetic resonance imaging.

Dr. Van De Ville served as an Associate Editor for the IEEE TRANS-ACTIONS ON IMAGE PROCESSING (2006-2009) and the IEEE SIGNAL PROCESSING LETTERS (2004-2006). He is a member of the Bio Imaging and Signal Processing (BISP) TC of the IEEE SPS. Since 2003, he has also been an Editor and Webmaster of The Wavelet Digest. He is a guest co-editor of the special issue on "Brain Decoding" in PATTERN RECOGNITION (2011). He is co-chair of the Wavelets series conferences (2007, 2009, 2011), together with V. Goyal and M. Papadakis.

Thierry Blu (M'96–SM'06) was born in Orléans, France, in 1964. He received the "Diplôme d'ingénieur" from École Polytechnique, France, in 1986 and from Télécom Paris (ENST), France, in 1988. In 1996, he obtained a Ph.D. in electrical engineering from ENST for a study on iterated rational filterbanks, applied to wideband audio coding.

Between 1998 and 2007, he was with the Biomedical Imaging Group at the Swiss Federal Institute of Technology (EPFL) in Lausanne, Switzerland. He is now a Professor in the Department of Electronic Engineering, The Chinese University of Hong Kong.

Dr. Blu was the recipient of two best paper awards from the IEEE Signal Processing Society (2003 and 2006). He is also coauthor of a paper that received a Young Author best paper award (2009) from the same society. Between 2002 and 2006, he has been an Associate Editor for the IEEE Transactions on Image Processing and since 2006, for the IEEE Transactions on Signal Processing. He is also Associate Editor of Elsevier Signal Processing and Eurasip J. on Image and Video Processing.

Research interests: (multi)wavelets, multiresolution analysis, multirate filterbanks, interpolation, approximation and sampling theory, sparse sampling, image denoising, psychoacoustics, biomedical imaging, optics, wave propagation

Brigitte Forster-Heinlein (M'04) received the diploma and doctoral degrees summa cum laude in mathematics from the Technische Universität München (TUM), Germany, in 1998 and 2001, respectively. From 2002–2004, she was a researcher in the Biomedical Imaging Group under M. Unser at the Swiss Federal Institute of Technology (EPFL), Lausanne, Switzerland. She is now a Junior Professor of mathematical modelling in biomedical engineering at TUM. In addition, she is team leader of the Marie Curie Excellence Team MAMEBIA, funded by the European Commission, at the Helmholtz Zentrum München-German Research Center for Environmental Health. Dr. Forster is member of the editoral board of the International Journal for Mathematics and Mathematical Sciences (IJMMS). Her main research topics are Dirichlet series, complex wavelets, and applications for signal and image processing.

Michael Unser (M'89–SM'94–F'99) received the M.S. (summa cum laude) and Ph.D. degrees in electrical engineering in 1981 and 1984, respectively, from the École Polytechnique Fédérale de Lausanne (EPFL), Switzerland.

From 1985 to 1997, he was a Scientist with the National Institutes of Health, Bethesda, MD. He is now full Professor and Director of the Biomedical Imaging Group, EPFL. His main research area is biomedical image processing. He has a strong interest in sampling theories, multiresolution algorithms, wavelets, and the use of splines for image processing. He has published over 150 journal papers on those topics and is one of ISIs Highly Cited authors in Engineering (http://isihighlycited.com).

Dr. Unser has held the position of associate Editor-in-Chief (2003–2005) for the IEEE TRANSACTIONS ON MEDICAL IMAGING and has served as Associate Editor for the same journal (1999–2002; 2006–2007), the IEEE TRANSACTIONS ON IMAGE PROCESSING (1992–1995), and the IEEE SIGNAL PROCESSING LETTERS (1994–1998). He co-organized the first IEEE International Symposium on Biomedical Imaging (ISBI2002). He was the founding chair of the technical committee of the IEEE-SP Society on Bio Imaging and Signal Processing (BISP). He received the 1995 and 2003 Best Paper Awards, the 2000 Magazine Award, and the 2008 Technical Achievement Award from the IEEE Signal Processing Society. He is an EURASIP Fellow and a member of the Swiss Academy of Engineering Sciences.